Biology of Reproduction, 2023, **109(5)**, 669–683
https://doi.org/10.1093/biolre/ioad093
Advance access publication date 8 August 2023
Research Article

Paxillin knockout in mouse granulosa cells increases fecundity†

Kenji Vann, Adelaide E. Weidner, Ariana C. Walczyk and Olga Astapova*

Division of Endocrinology, Department of Medicine, University of Rochester Medical Center, Rochester, NY, USA

***Correspondence:** University of Rochester Medical Center, Department of Medicine, Division of Endocrinology, 601 Elmwood Ave, Box 693, Rochester, NY 14642, USA. Tel: +15852752901; Fax: 585-320-1091; E-mail: olga_astapova@urmc.rochester.edu

†**Grant Support:** This work was supported by National Institutes of Health NICHD (Award Number 1K08HD107134-01A1) and University of Rochester Department of Medicine Pilot Award Program

Abstract

Paxillin is an intracellular adaptor protein involved in focal adhesions, cell response to stress, steroid signaling, and apoptosis in reproductive tissues. To investigate the role of paxillin in granulosa cells, we created a granulosa-specific paxillin knockout mouse model using Cre recombinase driven by the Anti-Müllerian hormone receptor 2 gene promoter. Female granulosa-specific paxillin knockout mice demonstrated increased fertility in later reproductive age, resulting in higher number of offspring when bred continuously up to 26 weeks of age. This was not due to increased numbers of estrous cycles, ovulated oocytes per cycle, or pups per litter, but this was due to shorter time to pregnancy and increased number of litters in the granulosa-specific paxillin knockout mice. The number of ovarian follicles was not significantly affected by the knockout at 30 weeks of age. Granulosa-specific paxillin knockout mice had slightly altered estrous cycles but no difference in circulating reproductive hormone levels. Knockout of paxillin using clustered regularly interspaced short palindromic repeat-associated protein 9 (CRISPR-Cas9) in human granulosa-derived immortalized KGN cells did not affect cell proliferation or migration. However, in cultured primary mouse granulosa cells, paxillin knockout reduced cell death under basal culture conditions. We conclude that paxillin knockout in granulosa cells increases female fecundity in older reproductive age mice, possibly by reducing granulosa cell death. This study implicates paxillin and its signaling network as potential granulosa cell targets in the management of age-related subfertility.

Summary Sentence

Granulosa cell-specific knockout of adaptor protein paxillin in mice leads to increased fecundity and may reduce granulosa cell death.

Graphical Abstract

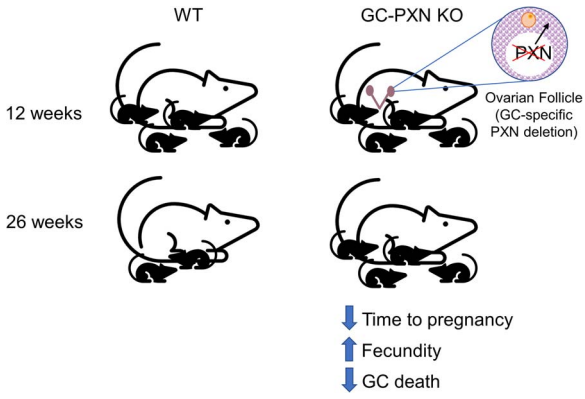

Key words: paxillin, granulosa, ovary, follicle, apoptosis, fecundity

Introduction

Reproductive aging and diminished ovarian reserve are increasingly important factors limiting female fertility as the mean age of childbearing rises in the USA [1]. Both germ cell factors, mainly oocyte aneuploidy [2, 3] and mitochondrial dysfunction [4, 5], and somatic ovarian cell factors have been implicated in subfertility with ovarian aging. Among the latter, granulosa cell oxidative stress has been shown to lead to accelerated primordial follicle depletion through apoptosis [6–9]. Increased apoptosis in the granulosa cells (GCs) of mature follicles has been linked to diminished ovarian reserve and poor outcomes in women undergoing in vitro fertilization [10–14]. Inflammation and mitochondrial dysfunction have been described alongside free radical damage in aging GCs [15–17]. These processes coalesce to result in reduced follicle survival years before the onset of menopause in normal

Received: January 23, 2023. **Revised:** May 29, 2023. **Accepted:** August 2, 2023

reproduction, or sooner in states of diminished ovarian reserve. However, cell-intrinsic factors that modulate these pathways are not well known.

The cytoplasmic adaptor protein paxillin is an integral part of the focal adhesion complex [18] and is also involved in apoptosis and oxidative stress response [19–21]. Paxillin serves many functions related to the cytoskeletal structure and cell signaling. It modulates extracellular matrix remodeling [22], regulates changes in the actin cytoskeleton [23], particularly in response to oxidative stress [21], and promotes intracellular kinase signaling [24]. Paxillin is regulated via phosphorylation by SRC proto-oncogene, non-receptor tyrosine kinase (SRC) and focal adhesion kinase (FAK), among others [20]. In many cancer cell models, paxillin is protective from apoptosis and is targeted by apoptotic caspases [25–28]. Its function in focal adhesions in particular protects from stretch-induced pathological signaling that can lead to apoptosis [29]. Although focal adhesions in GCs have not been studied in depth, some studies suggest that they are important in GC-oocyte communication [30] and ovulation [31] and are involved in GC apoptosis [32]. Recent studies have implicated paxillin in steroid signaling pathways in reproductive tissues, particularly androgen signaling in prostate cancer cells, where paxillin enhances both intranuclear androgen receptor transcriptional activity [24] and extranuclear androgen receptor transactivation of mitogen-activated protein (MAP) kinase signaling pathways [33–36].

There are very few studies on the role of paxillin in GCs and in female fertility. In one study, paxillin was found to play a role in mouse GC proliferation and apoptosis by promoting the transcription of an androgen-responsive anti-apoptotic microRNA, miR-125b, and by increasing the expression of follicle-stimulating hormone receptor [37]. Another study found that FYN proto-oncogene, Src family tyrosine kinase (FYN), a protein that interacts with paxillin within focal adhesions, is required for GC migration during ovulation, and disruption of FYN reduces ovulated oocytes in mice [38]. Given the established and emerging evidence of paxillin in processes that are important in GCs, including apoptosis, oxidative stress, focal adhesion formation, and steroid signaling, we hypothesized that paxillin in GCs is necessary for female fertility.

We predicted that paxillin loss in GCs would reduce cell proliferation and result in accelerated follicle loss with age; surprisingly, we found the opposite. Mice with GC-specific paxillin knockout (GC-PXN KO) exhibited increased fertility in later reproductive age through a complex phenotype involving altered estrous cycles. Paxillin-deficient GCs exhibited reduced cell death under basal in vitro culture conditions, suggesting that reduced paxillin expression may have a protective effect in GCs of older mice. Our findings suggest that paxillin is an important regulator of female fertility and may be implicated in ovarian aging.

Materials and methods

Generation of GC-PXN KO mice

Mouse studies were performed in accordance with the guidelines for the Care and Use of Laboratory Animals and were approved by the University Committee on Animal Resources at the University of Rochester (animal welfare assurance number D16-00188, approval date 07-12-2021). All experimental mice had the C57BL/6J genetic background achieved by back-crossing to C57BL/6J background mice for more than four generations. GC-PXN KO mice were generated by crossing mice with LoxP sites flanking exons 2–5 of the paxillin gene, obtained from Christopher Turner (Upstate Medical University) [39] with mice expressing Cre recombinase driven by the Anti-Müllerian hormone receptor type 2 (Amhr2) gene promoter obtained from Carolina Jorgez (Baylor College of Medicine) [40]. Tail DNA was extracted using Extracta DNA Prep for PCR (Quantabio) and genotyped using AccuStart II PCR Genotyping Kit (Quantabio) with PCR primers flanking the paxillin LoxP sites (upstream site: TACAGCTAAGGCATGTAGAG and GTTTGGGGCTGCACTCTACC, downstream site: ACGGGATGAGACGACATAGG and TACAGCGCTGCACATAGACG) and Amhr2-cre transgene (CCGCTTCCTCGTGCTTTACGGTAT and ACCTAGTAGAGAGGCTGCGTTGAGTGTG). Paxillin gene recombination occurred in the GCs, but not in peripheral tissues of Cre-positive, paxillin-floxed mice (Figure S1). Mice positive for Amhr2-cre and two paxillin-floxed alleles ($Amhr2^{Cre/+}$; $Pxn^{fl/fl}$) were considered GC-PXN KO, whereas mice negative for Amhr2-cre and positive for two paxillin-floxed alleles ($Amhr2^{+/+}$; $Pxn^{fl/fl}$) were designated as controls. To generate mice for the experiments, a GC-PXN KO female was crossed with a paxillin-floxed male from a different line of mice. Each experiment used mice from several litters, and cre-negative littermates served as controls.

Continuous breeding study

Female mice were bred continuously starting at 9 weeks of age with fertility-proven males <30 weeks of age. When the males reached 30 weeks of age, they were replaced with younger fertility-proven males. Pups were counted and sacrificed at birth, and maternal age was rounded up or down to the nearest week. Cumulative number of pups per female (six mice per group) was analyzed at 2-week intervals. The study was concluded at 26 weeks due to signs of mouse stress, including cannibalism of the neonates, which was attributed to the physiological pressure of continuous breeding. These signs were observed equally among control and knockout mice. In a separate cohort, 20-week-old females ($n = 3$ controls and 3 GC-PXN KO) were paired with wild-type fertility-proven males for up to 10 weeks of continuous breeding. Time to pregnancy was calculated as the number of days from one litter to the next litter minus 19 (the length of gestation). In this cohort, all mice experienced fetal dystocia complicating delivery of one of their litters and had to be euthanized.

Estrous cycle study

Estrous cycles were monitored using daily vaginal cytology as previously described [41] for 3 weeks in 24-week-old mice. Briefly, vaginal lavage samples were collected by repeatedly pipetting a drop of sterile phosphate-buffered saline at the vaginal opening, placed on a microscope slide and air dried. Slides were then processed using Hema 3 Stat Pack (Fisher Catalog No. 22-122911) according to manufacturer's instructions and visualized under light microscopy. Similarly to a previously developed protocol [42], samples containing predominantly neutrophils were classified as diestrus, samples where at least a third of the cells were nucleated epithelial cells were classified as proestrus, samples with only epithelial cells (both nucleated and keratinized) were classified as estrus, and samples containing both keratinized epithelial cells and neutrophils were classified as metestrus.

Follicle counting

Mice were euthanized at 30 weeks. Ovaries were fixed in formalin and stored in 70% ethanol until processing. Entire ovaries were embedded in paraffin, sectioned at 8-um thickness, and stained with hematoxylin and eosin. Follicles were identified in every fifth section by visual inspection under light microscopy and classified as previously described [43]. Briefly, primary follicles contained a single layer of cuboidal GCs, secondary follicles contained more than one layer of GCs and no antrum, antral follicles contained an antral space surrounding less than half of the oocyte diameter, preovulatory follicles contained an antrum that surrounded more than half of the oocyte diameter, atretic follicles contained degenerating oocytes with fragmented zonae pellucidae, and corpora lutea contained luteinized cells with abundant cytoplasm and no oocyte. All follicles were counted by a single observer, who was blinded to the mouse genotype. Primordial follicles counted in eight sections for each mouse, and total number of primordial follicles was estimated based on total number of sections for each mouse.

Ovulation counting

After completion of the continuous breeding study, estrous cycles were monitored daily as described under "Estrous Cycle studies." Once resumption of cycles was confirmed, the mice were sacrificed on the first day of estrus within the second or third cycle, at age 28–30 weeks. Oviducts were dissected and placed in phospho-buffered saline. Ovulated oocyte-containing ampullae were identified under a dissecting microscope, and the cumulus-oocyte mass was released into a solution of 0.5 mg/mL hyaluronidase and observed for dispersion, then oocytes were counted and the total number from both sides of each mouse was recorded.

Circulating hormone measurements

The 28–30-week-old mice were sacrificed on the first day of estrus, as described under "Ovulation counting." Whole blood was collected from the inferior vena cava immediately after euthanasia, incubated at room temperature for 30 min, and centrifuged at 1000 g for 15 min. Serum was aspirated and stored at −80°C until analysis. Samples were analyzed by the Ligand Assay and Analysis Core Laboratory at the University of Virginia, Charlottesville, VA. All assays were done using mouse and rat ELISA. Samples were diluted 1:10 for luteinizing hormone (LH) and follicle stimulating hormone (FSH) assays. The detection ranges were as follows: 0.016–4.0 ng/mL for LH, 0.016–8.0 ng/mL for FSH, 5.0–3200.0 pg/mL for estradiol, 10.0–1600.0 ng/dL for testosterone, and 21.15–1350.0 ng/mL for Anti-Müllerian hormone (AMH). Two samples were below the estradiol detection range, and the lowest detectable value of 5 pg/mL was used for those data points (one control and one GC-PXN KO).

Immunohistochemistry

Ovaries from 15-week-old mice were processed and sectioned as described under "Follicle counting," then deparaffinized in xylene and ethanol. Antigen retrieval was done by boiling the samples in 10 mM citrate (pH 6.0) for 10 min at 20% power in a microwave. Endogenous peroxidase activity was quenched in 3% hydrogen peroxide. Sections were blocked in 2.5% horse serum before incubation with rabbit anti-paxillin IgG (Abcam Catalog No. 32115, RRID: AB_777116, 1:25 dilution) overnight at 4°C, followed by biotinylated goat anti-rabbit IgG (Vector Laboratories Catalog No. BA-1000, RRID: AB_2313606, 1:200) for 2 h at room temperature. Signal was developed using the VECTASTAIN Elite ABC-HRP kit (Vector Laboratories Catalog No. PK-6100) and Vector DAB peroxidase substrate (Vector Laboratories Catalog No. SK-4100). Samples were counterstained with hematoxylin, dehydrated with ethanol and xylene, then mounted with VectaMount (Vector Laboratories Catalog No. H-5000-60).

Cell culture

To culture primary GCs, ovaries from 24- to 26-week-old mice were dissected in phosphate-buffered saline, then transferred to Dulbecco modified Eagle medium (DMEM)/F12 (Invitrogen Catalog No. 11330-057). Follicles were punctured under a dissecting microscope with 31-gage needles to extrude GCs into the media, as previously described [44]. Cells were pelleted at 1000 g for 5 min, then resuspended in fresh DMEM/F12 supplemented with 10% fetal bovine serum (FBS) and cultured at 37°C and 5% CO2 for up to 4 days.

KGN cells were obtained from RIKEN (RRID: CVCL_0375) and cultured in DMEM/F12 supplemented with 10% FBS at 37°C and 5% CO2. Cells were passaged every 5–6 days, and passage number <20 was used for experiments.

Generation of paxillin-knockout KGN cells

KGN cells were transfected using jetPRIME (Polyplus) with an all-in-one non-viral vector set containing three sgRNAs for the human paxillin gene (ABM Catalog No. 382401110591) or non-coding control vector. Two days later, green fluorescent protein-positive cells were selected using BioRad S3e flow cytometer and seeded into a 96-well at 1 cell per well to generate single cell-derived clones. Paxillin knockout was confirmed by western blot, and six clones each of knockout and control cells were selected for experiments.

Western blotting

Western blotting was performed as previously described [45]. Briefly, cells were suspended in lysis buffer containing 50-mM Tris base, 150-mM NaCl, 5-mM EDTA, 1% Triton X-100, and protease and phosphatase inhibitor cocktail (Halt, Thermo Catalog No. 1861281). Cell lysates were boiled for 5 min in sample buffer containing 5% β-mercaptoethanol, then separated in sodium dodecyl sulfate–polyacrylamide gels 4–15% gradient gels and transferred onto polyvinylidene fluoride membranes in 20% methanol. Blots were blocked for 1 h at room temperature with 5% milk in Tris-buffered saline with 0.1% Tween, then probed overnight at 4°C with primary antibodies (paxillin: BD Biosciences 610051, RRID:AB_397463, 1:1000; GAPDH: Cell Signaling Technology 2118, RRID:AB_561053, 1:4000; Caspase-3 (validated to detect uncleaved and cleaved Caspase-3): Cell Signaling Technology 9662, RRID:AB_331439, 1:1000; Caspase-9 (validated to detect uncleaved and cleaved Caspase-9): Cell Signaling Technology 9508, RRID:AB_2068620, 1:1000; transforming growth factor beta 1 induced transcript 1 (TGFB1I1, Hic-5): BD Biosciences 611165, RRID: AB_398703, 1:1000; Fyn: Cell Signaling 4023, RRID: AB_10698604, 1:1000; cytochrome P450, family 19 (Cyp19): ThermoFisher BS-1292R, RRID: AB_10880885, 1:1000), followed by secondary antibodies for 1 h at room temperature (mouse: BIO-RAD Catalog No. 170-6516, RRID:AB_11125547, 1:5000; rabbit: BIO-RAD Catalog No. 1706515, RRID:AB_11125142, 1:5000). Band density was quantified using ImageJ [46] and normalized to GAPDH.

Cell migration assays

Paxillin-knockout and control KGN cells were seeded at 100 000 cells/well in a 200 μL volume of serum-free DMEM/F12 in Transwell permeable supports (6.5 mm diameter and 8 μm pore size, Corning Catalog No. 3422) in 24-transwell dishes. In the bottom chamber, 750 μL of DMEM/F12 supplemented with 10% FBS was added. After 24 h, cells were fixed and stained with 0.5% of crystal violet (Sigma). Cells that migrated across the well were imaged using Olympus IX71 inverted microscope and counted using ImageJ [46].

Cell proliferation assays

Paxillin-knockout and control KGN cells were seeded in 96-well plate at 2000 cells/well in DMEM/F12 supplemented with 10% FBS. For BrdU assays, after 3 days of culture, 10 μM BrdU was added to the plate and cells were incubated for 24 h. Cell proliferation was assessed using the BrdU Cell Proliferation Assay Kit (Cell Signaling Technology Catalog No. 6813). For MTT (3-(4,5-dimethylthiazol-2-yl)-2,5-diphenyltetrazolium bromide) metabolism assays, after 3 days of culture, the Cell Proliferation Kit I (MTT) protocol (Millipore Sigma Catalog No. 11465007001) was carried out as per manufacturer's instructions.

TUNEL assays

Ovaries from 24-week-old mice were preserved and sectioned as described under "Follicle counting." Primary GCs were collected from 24- to 26 -week-old mice as described under "Cell culture" and plated on poly-L-lysine-treated glass coverslips. After 4 days in culture, cells were treated with 1 mM hydrogen peroxide for 4 h and fixed with 4% paraformaldehyde. TUNEL assays on ovary sections and primary cells were performed using the Click-iT kit (ThermoFisher Catalog No. C10245) according to manufacturer instructions. Samples were mounted in Duolink In Situ Mounting Medium with DAPI (4′, 6-diamidino-2-phenylindole; Sigma Catalog No. DUO82040). Five follicles from each ovary or five high-power fields (HPFs) from each primary cell culture sample were imaged using a fluorescent microscope, and fluorescence was quantified using ImageJ [46]. Total fluorescence was adjusted to the area of each follicle or to the number of cells in each image of primary cells.

Immunofluorescence

Ovarian sections and primary GCs were prepared as described in "TUNEL assays," without hydrogen peroxide treatment. After fixation, ovarian sections underwent heat antigen retrieval, were permeabilized, blocked and washed as previously described [47]. Fixed primary GCs were permeabilized with 0.25% Triton X-100 and blocked with 2% bovine serum albumin. Samples were then probed with primary antibodies (paxillin: BD Biosciences 610051, RRID: AB_397463, 1:100; vinculin: Proteintech 26520-1-AP, RRID: AB_2868558, 1:100) overnight at 4°C. Secondary antibodies were applied for 2 h at room temperature in the dark (Texas Red goat anti-rabbit: ThermoFisher T-2767, RRID: AB_2556776, 1:500; FITC goat anti-mouse: ThermoFisher F-2761, RRID: AB_2536524, 1:500). Samples were mounted in Duolink In Situ Mounting Medium with DAPI (4′, 6-diamidino-2-phenylindole; Sigma DUO82040). Validation of these antibodies is shown in Figure S2.

Quantitative PCR

Primary GCs were cultured as described above for 4 days, then total RNA was isolated with TRIzol (ThermoFisher 15596026) according to the manufacturer's instructions. The 1 μg of RNA was used to synthesize complementary DNA with the qScript cDNA Synthesis Kit (Quantabio 95047), and the cDNA was then used to quantify specific transcripts using the PerfeCTa SYBR Green SuperMix (Quantabio 95056). The following primers were used for the quantitative PCR reactions: Cyp19 (F: GCATCGGCATGCATGAGAAC; R: CATTCGAACAAGACCAGGGC), Taf4b (F: TCGCCTCAGCAAGCTGTAAC; R: CAGGCGCCACTGTTACTTTC), Grem2 (F: AGAGTGACTGGTGCAAGACG; R: GTCGCGGGATGTAGAAGGAG), and Ar (F: TGACAAGCCAGGAGAGTGAC; R: GTACAATCGTTTCTGCTGGCAC).

Statistical analyses

Data are shown as averages and standard errors. All data analysis was done using GraphPad Prism. Unless otherwise indicated, groups were compared using two-tailed t test. Serum hormone ELISA data were analyzed by non-parametric Mann–Whitney test. For the serum hormone assay data, due to a wide intra-group variability, outlier analysis was performed using ROUT with Q = 5%. As a result, two samples were excluded from analysis of estradiol levels (one control and one GC-PXN KO) as outliers.

Results

Confirmation of paxillin knockout in mouse GCs

To examine the role of paxillin in GCs, we generated GC-PXN KO mice by breeding mice expressing Cre recombinase driven by the Anti-Müllerian hormone receptor 2 gene promoter with mice whose paxillin gene contains LoxP sites flanking paxillin gene exons 2–5. Paxillin knockout was confirmed by immunohistochemistry in 15-week-old mouse ovaries. As shown in Figure 1, knockout (GC-PXN KO: $Amhr2^{Cre/+}$; $Pxn^{fl/fl}$) females demonstrated loss of paxillin expression in GCs, compared with their littermate controls ($Amhr2^{+/+}$; $Pxn^{fl/fl}$), where paxillin expression was detected in all ovarian cell types. Paxillin expression in theca cells was not affected (Figure 1B), confirming the GC specificity of paxillin knockout in our mouse model. A small amount of residual paxillin expression was observed in cultured primary PXN-knockout GCs, which we attribute to the long half-life of paxillin protein (longer than 4 days in our experiments, Figure S3). This may also be due to mosaicism in Cre expression when driven by the Amhr2 gene promoter.

Increased fecundity in GC-PXN KO mice

To determine the effect of GC-specific paxillin loss on female fertility, we performed a continuous breeding study. Control and knockout females were paired with proven-fertile, reproductive age males starting at 9 weeks of age. Each resulting litter was counted, and the pups were sacrificed on postnatal day 1. As shown in Figure 2A and B, control and knockout females produced similar offspring numbers early in their reproductive life. However, by mid-reproductive age, approximately week 25, control females began to produce fewer pups, whereas knockout mice continued to produce pups at the same rate as earlier in life. As a result, there was a

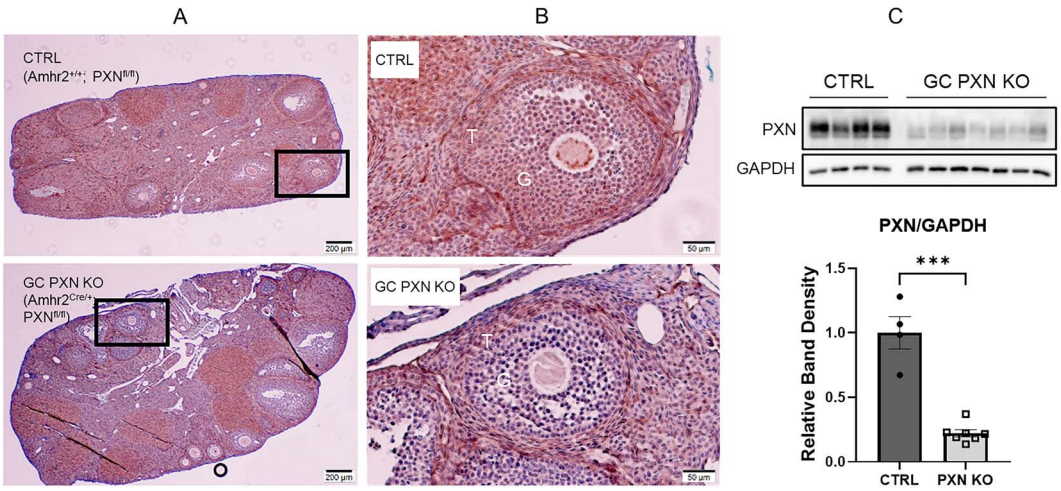

Figure 1. Reduced paxillin expression in granulosa-specific PXN knockout mice. (A) Immunohistochemistry of PXN expression (brown) in hematoxylin-counterstained ovarian sections (blue). (B) Magnified images of early antral follicles indicated in panel A. G, granulosa cells; T, theca cells. (C) Paxillin protein expression measured by western blot (top) and band densitometry (bottom) in cultured primary mouse GCs. $^{***}P < 0.001$.

significant increase in the total number of pups per female by age 24–26 weeks, in other words fecundity was increased in GC-PXN KO females. This was due to an increased number of litters (Figure 2C), while the number of ovulated oocytes per cycle and the number of pups per litter were not affected by the knockout (Figure 2D and E). Consistent with the increased number of litters at older age, the time to pregnancy, measured in days between delivery and conception at ages 24–28 weeks, was significantly shorter in knockout females (Figure 2F). Time to pregnancy was similar before 24 weeks (data not shown).

Altered estrous cycles in GC-PXN KO mice

To determine whether the observed increase in litter frequency was due to increased estrous cycle frequency and/or increased time in estrus, we monitored the estrous cycles in control and GC-PXN KO females at 24–27 weeks of age by daily vaginal lavage. Representative cycle profiles are shown in Figure 3A. The number of cycles was similar in control and knockout females (Figure 3B). However, within each cycle, the knockout females spent significantly less time in estrus and more time in diestrus (Figure 3C and D). These results suggest that the observed effect of PXN knockout of female fecundity is neither due to increased time spent in the receptive and fertile stages of the estrous cycle later in life nor due to increased frequency of estrous cycles later in life.

Follicle numbers are not significantly affected by GC-PXN KO

To estimate the ovarian reserve of GC-specific PXN knockout mice, we determined the total number of follicles in both ovaries of each female at age 28–30 weeks. Total number of follicles was not significantly different between the two groups, likely due to high within-group variability (Figure 4A). When the follicles were grouped into developmental stages, the average number of follicles at each stage was higher in the knockout mice, but there was no significant effect of the genotype in multiple ANOVA, and these differences were not statistically significant in post hoc analyses (Figure 4B).

GC-PXN KO does not affect circulating reproductive hormone levels

To investigate whether the GC paxillin knockout disrupted the pituitary-gonadal axis hormone homeostasis, circulating hormone levels were measured on the first day of estrus in mice aged 28–30 weeks. There were no statistically significant differences in the serum levels of LH, FSH, estradiol, or testosterone (Figure 5). These data indicate that GC-PXN KO does not result in significant differences in pituitary or ovarian hormone production. To further characterize the follicle reserve in the knockout mice, we measured AMH levels, which correlates with the primordial follicle pool in mice [48]. There was no statistically significant difference in serum AMH levels between control and knockout mice (Figure 5).

Paxillin knockout in KGN cell does not affect cell proliferation and migration

Paxillin has been implicated in the proliferation and migration of many cancer cells, including prostate cancer. These cell functions in GCs may affect ovarian follicle reserve, contributing to the observed phenotype in our mouse model. To investigate whether paxillin knockout affected GC proliferation and/or migration, we measured these parameters in KGN cells with CRISPR-generated PXN gene deletion. This immortalized human granulosa-derived cell model was chosen as a substitute for primary mouse GCs, in which cell number is technically challenging to quantify due to cell–cell adhesion within the cumulus-oocyte complex. As shown in Figure 6, PXN-targeted sgRNA transfection resulted in the generation of six PXN-null KGN clones derived from single cells. PXN gene deletion did not alter the proliferation of KGN cells, measured by DNA synthesis (BrdU incorporation) or mitochondrial metabolism (MTT) assays. Similarly, cell migration measured using the Transwell method was not affected by PXN loss in KGN cells.

Paxillin knockout reduces primary GC death

The GC death through apoptosis and other pathways has been linked to ovarian follicle depletion and the timing of menopause. To evaluate the effect of paxillin knockout on GC survival in the GC-PXN KO mice, we measured apoptotic

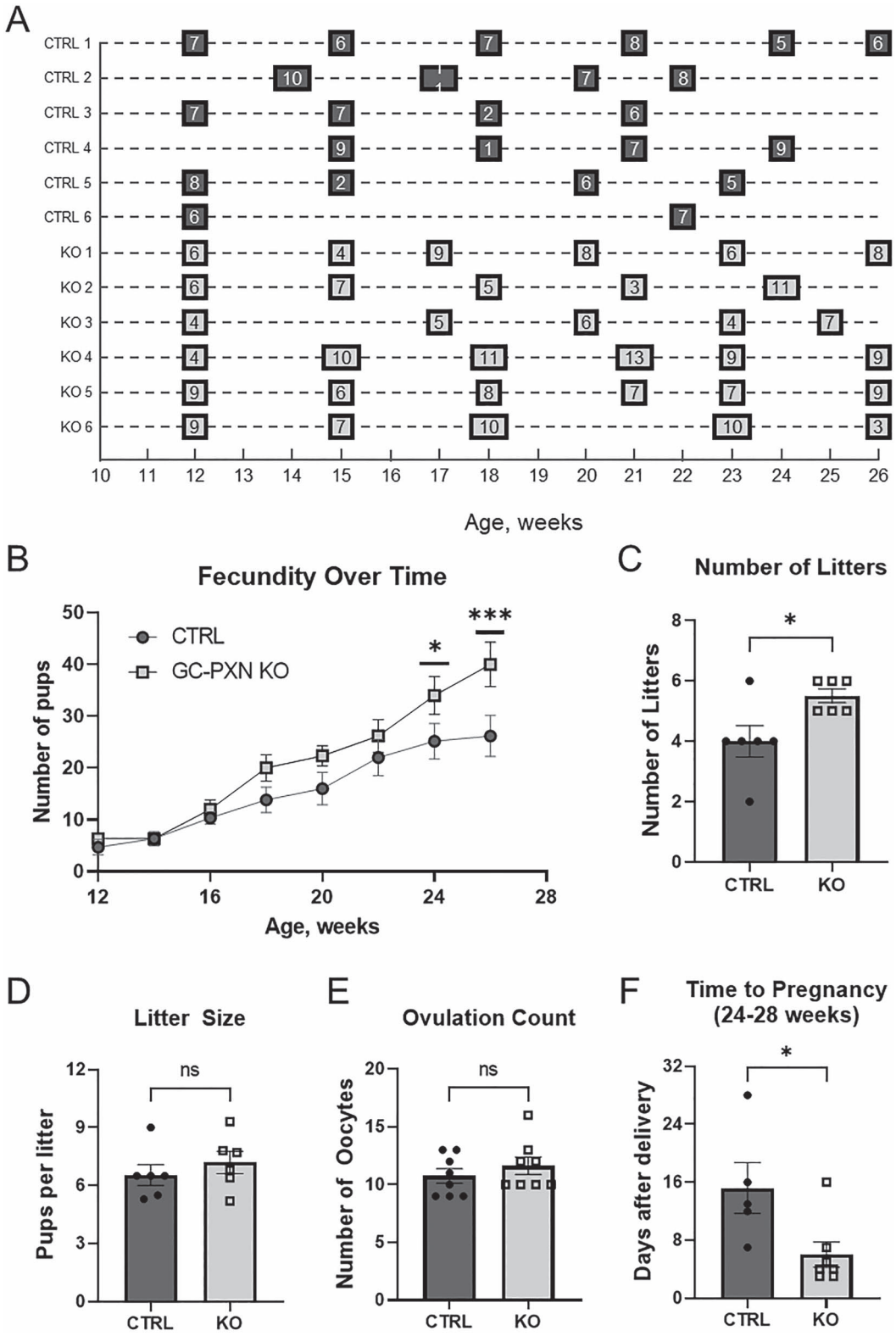

Figure 2. Granulosa-specific PXN knockout mice produce more pups when bred continuously to 26 weeks of age due to increased number of litters over time. (A) Schematic representation of litter appearance and size for each mouse in the study. (B) Cumulative number of offspring per female ($n = 6$ per group) from 12 to 26 weeks of age. (C) Total number of litters per female ($n = 6$ per group) from 12 to 26 weeks of age. (D) Average size of all litters produced by each female ($n = 6$ per group) between 12 and 26 weeks of age. (E) Number of oocytes counted in both ampullae during estrus at 28–30 weeks of age ($n = 8$ per group). (F) Number of days between delivery and subsequent pregnancy observed between 24 and 28 weeks of age in a separate cohort (CTRL: $n = 5$ litters by three mice; PXN-KO: $n = 7$ litters by three mice). Graphs represent averages and standard errors. ns, not significant. $^{*}P < 0.05$, $^{***}P < 0.001$.

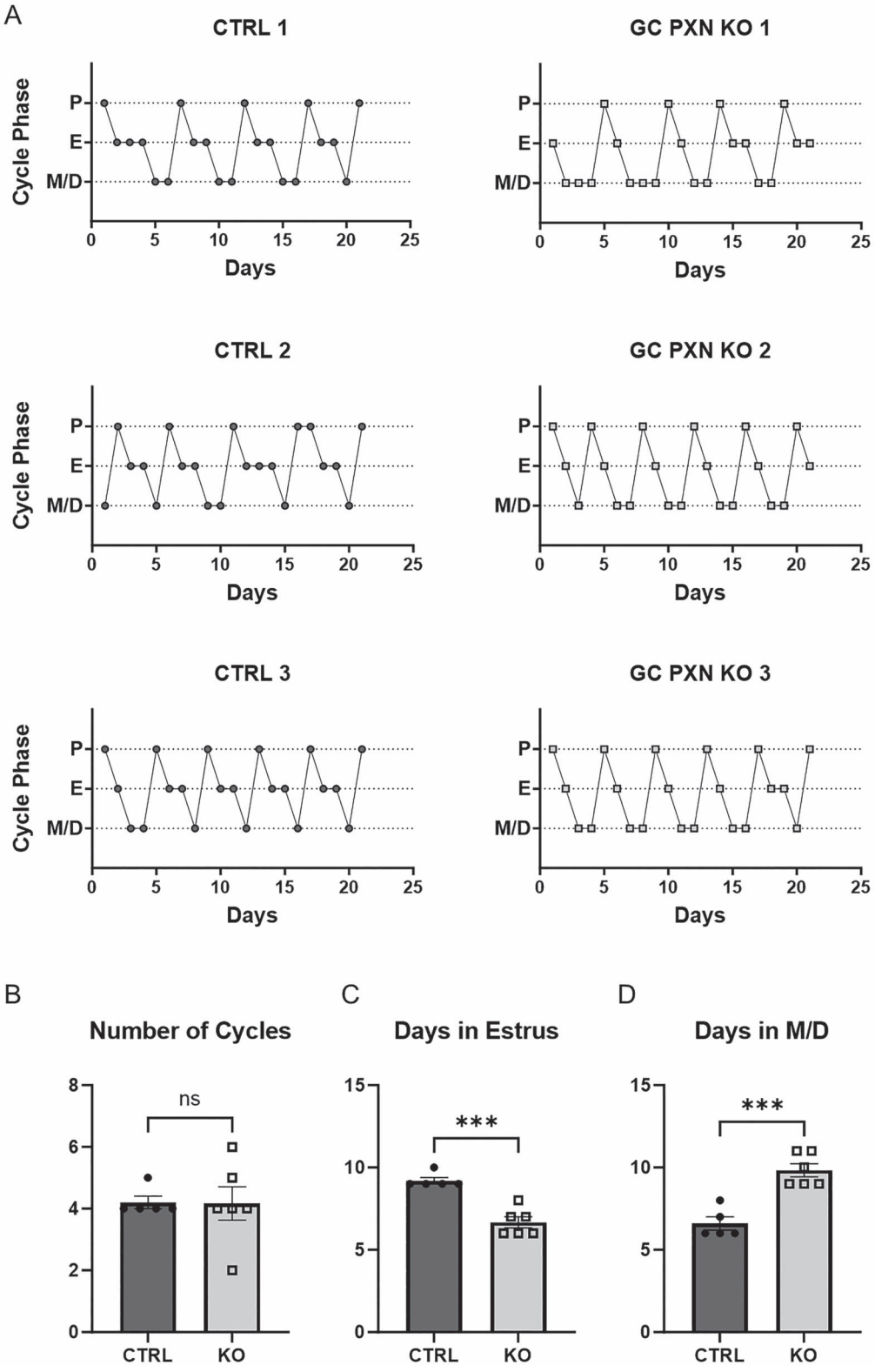

Figure 3. Granulosa-specific PXN knockout mice spend less time in estrus and more time in diestrus and metestrus. (A) Representative estrous cycle charts of three CTRL and three GC-PXN KO mice. P, proestrus; E, estrus; M/D, metestrus or diestrus. (B) Number of cycles, defined as proestrus followed by estrus, observed over 21 days. (C) Total number of days spent in estrus over 21 days. (D) Total number of days spent in metestrus and diestrus over 21 days. Graphs represent averages and standard errors (CTRL: $n = 5$, PXN-KO: $n = 6$). ns, not significant. $^{***}P < 0.001$.

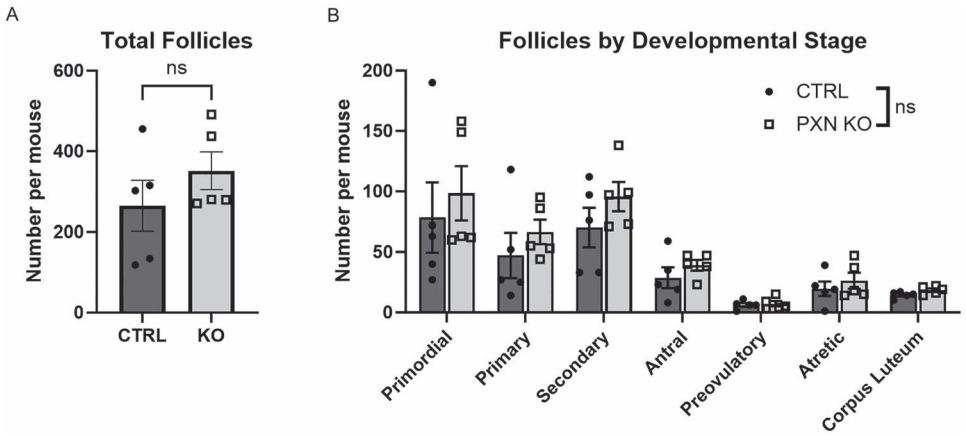

Figure 4. Follicle counts from both ovaries of 28–30 week-old control (CTRL) and GC-PXN KO (KO) mice ($n = 5$ mice per group). (A) Total follicle number in both ovaries. (B) Follicles grouped by developmental stage compared by multiple ANOVA. ns, not significant for the main effect of genotype (CTRL vs. KO).

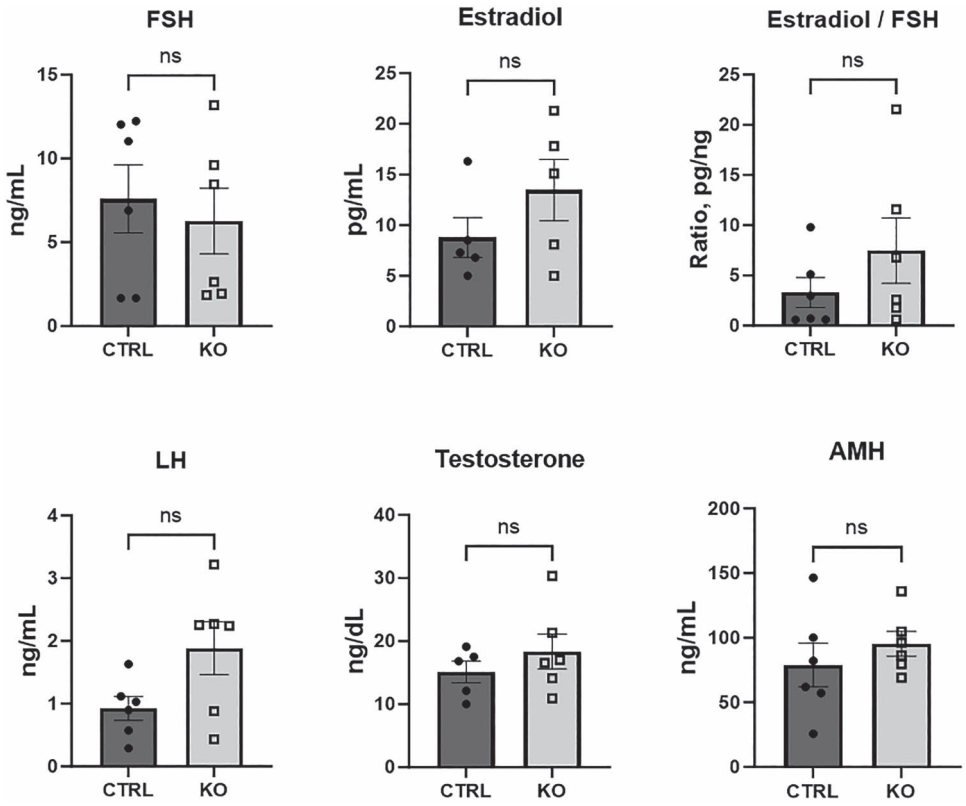

Figure 5. Serum hormone levels in 30-week-old control (CTRL) and GC-PXN KO (KO) mice during estrus. FSH, follicle stimulating hormone; LH, luteinizing hormone; AMH, anti-mullerian hormone. Graphs represent averages and standard errors of five to six mice per group, after removal of outliers. ns, not significant.

cell death using TUNEL assay in whole ovary sections and in cultured primary GCs isolated from 24- to 26-week-old mice. In whole ovaries, follicle apoptosis was lower than stromal apoptosis, and there was no difference in follicle apoptosis between CTRL and PXN KO groups. In primary GCs cultured in vitro for 4 days, nuclear TUNEL signal was absent under basal conditions and induced by treatment with 1 mM peroxide for 4 h, indicating breakage of double-stranded DNA due to oxidative stress-induced apoptosis (Figure 7). However, cells grown under basal conditions demonstrated cytoplasmic TUNEL signal, which has been attributed to cell death through necrosis and necroptosis, a programmed form of necrosis [49]. This basal TUNEL signal was significantly lower in PXN-KO GCs, suggesting that paxillin knockout improves survival of GCs in older mice, and this may contribute to the increase in fertility observed in this model. Peroxide-induced apoptosis was similar in control and PXN-KO GCs, indicating that paxillin loss does not affect cell survival in the face of severe oxidative stress. Protein expression of apoptotic caspases 3 and 9, as well as Hic-5, an apoptotic factor regulated by paxillin, was not affected by paxillin knockout in cultured GCs in either basal or peroxide-treated

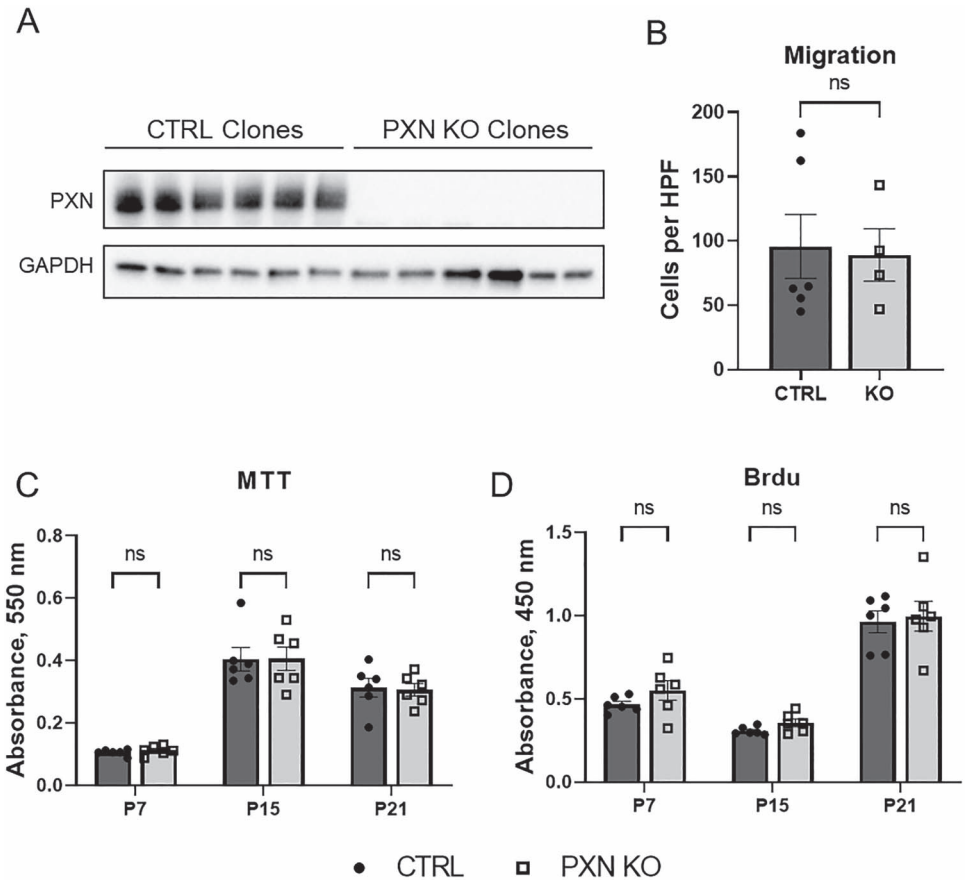

Figure 6. PXN knockout in human granulosa-derived KGN cells does not affect cell proliferation, migration, or metabolic activity. (A) Western blot of PXN expression in control (CTRL) and PXN knockout (PXN KO) clonal cell lines generated by CRISPR-Cas9 deletion of the PXN gene. (B) Number of cells per HPF migrated through a Transwell over 24 h, average of six CTRL and four PXN KO clones. (C) Quantification of metabolically active cells by measurement of conversion of 3-(4,5-dimethylthiazol-2-yl)-2,5-diphenyltetrazolium bromide (MTT) to formazan. (D) Measurement of cell division by Bromodeoxyuridine (BrdU) DNA incorporation assay. For C and D, CTRL and PXN KO KGN cells taken during early (P7, passage number 7), middle (P15, passage number 15), or late (P21, passage number 21) stages of cell culture were assayed after 3 days of growth in 96-well plates, averages of six CTRL and KO clones. ns, not significant.

conditions (Figure 7C and D). Cleaved caspase expression was not detected in untreated GCs, whereas procaspase expression was similar in control and PXN-KO GCs (Figure 7C), suggesting that the effect of paxillin knockout in untreated GCs is not through the classical apoptosis pathway.

Paxillin knockout does not abrogate focal adhesions in GCs

Considering paxillin's recognized role in focal adhesion formation and maintenance, we examined the expression and localization of vinculin, a marker of focal adhesions, in PXN-KO GCs. Immunofluorescence of ovarian sections from 24-week-old mice showed that, while paxillin expression was reduced expected in follicles of PXN-KO mice, vinculin expression was not affected (Figure 8A). Vinculin was detected outside the nucleus, as was paxillin in wild-type follicles, but distinct membrane structures representing adhesion foci were not observed. To examine focal adhesions in an environment that requires adhesion, we cultured primary GCs and repeat the immunofluorescence study. In this context, paxillin and vinculin colocalized within distinct membrane structures most likely representing focal adhesions in control GCs (Figure 8B). Paxillin expression within focal adhesions was significantly reduced or completely lost in PXN-KO GCs; however, vinculin expression pattern was not significantly altered. We conclude that PXN-KO GCs are able to form adhesion junctions in a monolayer culture, but the role of these structured in vivo requires further investigation. Likewise, the protein and mRNA expression of GC marker Cyp19 was not affected by PXN knockout (Figure 8C and Figure S4).

Discussion

We showed for the first time that knockout of paxillin using the Amhr2 gene promoter results in specific reduction of paxillin expression in GCs. Due to the long half-life of paxillin protein and other potential factors, including mosaicism, some of its expression persisted throughout follicular development, even after the gene recombination event. We observed that follicles developed normally in the face of this sub-total loss of paxillin; it is unknown how a complete loss of paxillin expression may affect follicle development and fertility. Paxillin is involved in the formation and maintenance of focal adhesion junctions and is closely associated with FAK, which is necessary for GC-oocyte communication through gap junctions and oocyte maturation [30]. It may be speculated that complete loss of paxillin would result in failure of oocyte

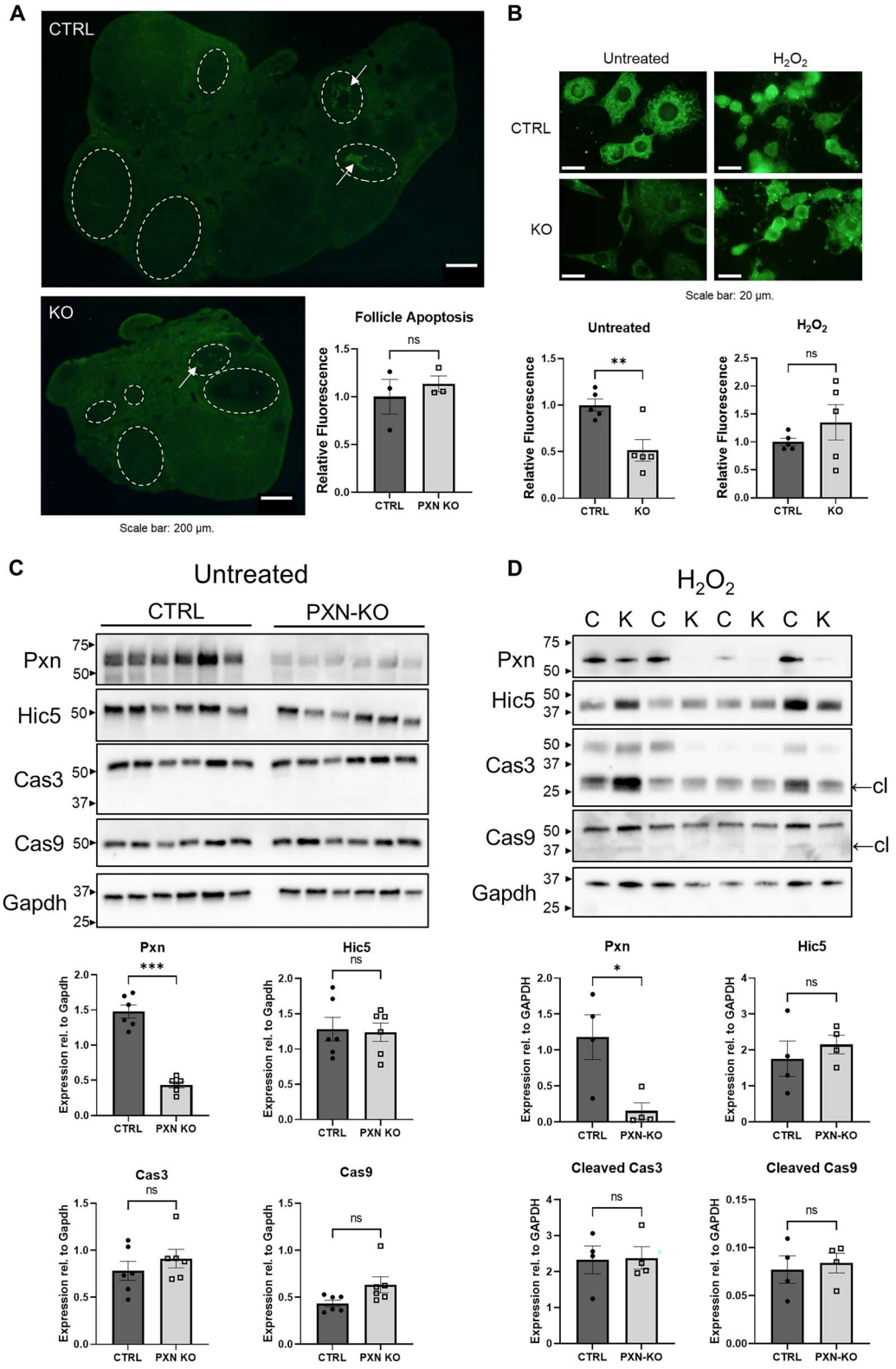

Figure 7. Cell death studies in PXN-deficient GCs. (A) Representative images and quantification of TUNEL immunofluorescence in whole ovary sections (one section per mouse) of 24-week-old control (CTRL) and GC-PXN KO (KO) mice. Fluorescence signals from five follicles, outlined in dashed lines, were normalized to follicle area and averaged for each mouse. Quantification is an average of three mice per group. White arrows point to areas of GC apoptosis. (B) Representative images and quantification of TUNEL immunofluorescence in cultured primary GCs from 24 to 26-week-old control (CTRL) and GC-PXN KO (KO) mice. Cells were grown for 4 days, then treated with 1 mM peroxide (H2O2) or left untreated. Total fluorescence per cell was determined in five HPFs for each sample. Quantifications are average of five mice per group. ns, not significant. $^{**}P < 0.01$. (C, D) Protein expression of apoptotic factors in untreated (C) and peroxide-treated (D) primary GCs treated as described in (B). cl, cleaved caspase bands. Band densitometry of the western blots is shown on the bottom ($n = 4$–6 mice per group).

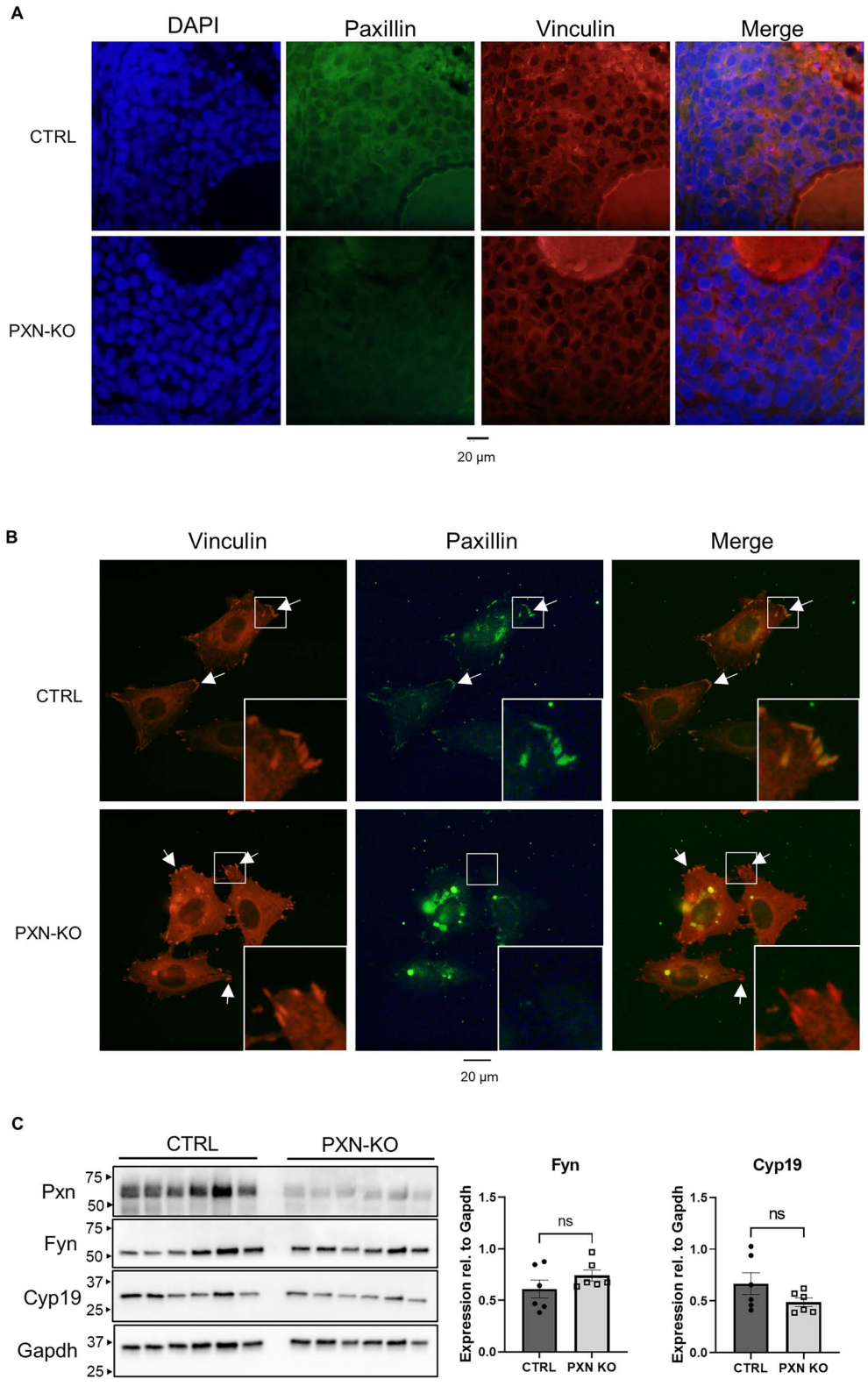

Figure 8. Immunofluorescence studies of paxillin and vinculin expression in PXN-KO GCs. (A) Representative images of large preantral follicles from 24-week-old control (CTRL) and GC-PXN KO (PXN-KO) mice immunostained for paxillin and vinculin. DAPI labels nuclei. Merge: combined DAPI, paxillin, and vinculin images. (B) Representative images of cultured primary GCs from control (CTRL) and GC-PXN KO (PXN-KO) mice at 24 weeks of age immunostained for paxillin and vinculin. Merge: combined paxillin and vinculin images. White arrows point to focal adhesions. Insets show magnified images of focal adhesions indicated in white boxes. (C) Protein expression and band densitometry of Fyn and Cyp19 in primary GCs from 24-week-old control (CTRL) and GC-PXN KO (PXN-KO) mice ($n = 6$ per group).

maturation due to disrupted gap junction functions. The apparent paxillin staining of corpora lutea in our GC-PXN KO model (Figure 1A) may be due to a large presence of non-granulosa lineage cells within these structures, such as theca-lutein cells, fibroblasts, endothelial cells, macrophages, and leukocytes, which in histological studies have been reported to represent the majority of cells within the corpus luteum [50].

Our GC-PXN KO female mice had similar reproductive metrics before 24 weeks of age, but exhibited increased fertility in later reproductive age due to shorter time to pregnancy and increased number of litters. Although our study was likely underpowered to detect a statistically significant difference in the number of follicles at any particular developmental stage, the average number of ovarian follicles at all stages of development was greater in the knockout mice. One limitation of this study is that follicles were counted only at one time point, when the reproductive phenotype became apparent. It is important to note that follicle counts in younger, prepubertal mice may be a better measure of ovarian reserve, and this information may have provided more insight into the mechanisms of paxillin in female fertility. Due to technical limitations, this was not done. To our knowledge, this is the first report of paxillin as a potential regulator of GC health and female fertility in older reproductive age. While we have not observed significant changes in paxillin expression in GCs over the reproductive lifespan, formal studies of this are warranted.

In our studies, measures of ovarian reserve, including the number of follicles and circulating AMH levels, were not affected by GC-PXN KO. To investigate other potential mechanisms through which PXN loss in GCs may affect fertility, we focused on GC-intrinsic factors: proliferation, migration, and cell death. In granulosa-derived human immortalized KGN cells, knockout of PXN did not affect cell proliferation or migration. We then assessed GC death in response to oxidative stress, a process that has been linked to ovarian aging and premature ovarian failure. In a mouse model, chronic oxidative stress through 30-day ozone exposure resulted in damage to GC membranes, reduced follicle quality, and reduced fertility [51]. The level of apoptosis in follicles in vivo was found to be quite low in our studies, and no differences were detected in GC-PXN KO mice. However, cultured primary mouse GCs in our studies began to undergo cell death demonstrated by cytoplasmic TUNEL signal after 4 days in culture. This pattern of TUNEL signal has been described in cells undergoing cell death through necrosis, characterized by leakage of some fragmented DNA into the cytoplasm [49]. Our results suggest that cultured mouse GCs begin to undergo necrosis after several days of in vitro growth. PXN knockout resulted in significantly less necrosis in this setting, indicating that PXN may promote basal necrosis in mouse GCs under these conditions.

On the other hand, when acute oxidative stress was introduced in cultured GCs, the rate of apoptosis measured by TUNEL assay was similar in control and PXN-KO cells. This is in contrast with the existing literature on paxillin's anti-apoptotic properties in various cancer cell models [52–55]. This difference may be due to fundamental differences between cancer and non-cancer cells, or it may be because the amount of oxidative stress due to peroxide treatment overwhelmed any protective effect from paxillin. In one study, FAK interacting with paxillin was shown to reduce chemically induced apoptosis, but not necrosis in renal tubular epithelial cells [56]. The FAK-paxillin signaling axis protects cells from apoptosis in the face of cell-damaging stress, but under basal conditions its role may be different. Our findings suggest that in GCs, paxillin promotes slow, chronic cell death through necrosis, but when the cell is overwhelmed by acute oxidative stress, it undergoes apoptosis regardless of the level of paxillin expression.

Not all of our findings are readily explained in the context of the reproductive phenotype induced by PXN knockout in GCs. We observed that GC-PXN KO mice spent less time in estrus, which appears counterintuitive to their enhanced fertility. Analysis of gonadal axis hormones in the serum revealed no significant changes in gonadotropins or sex steroid levels in our GC-PXN KO mice suggesting that the pituitary-ovarian hormone signaling axis was intact. However, Amhr2 expression has been reported in hypothalamic GnRH-producing neurons [57] and in the uterus [58, 59], suggesting that PXN knockout using the Amhr2 promoter-driven Cre expression may affect reproductive tissues outside of the ovary. These changes, which are not directly explored in our studies, may explain the estrous cycle differences and the reproductive phenotype of our knockout model. Measuring hormone levels during diestrus would have been helpful to assess baseline hormone dynamics in our mouse model. Many experts have voiced concerns over inaccuracies with the measurement of estradiol using ELISA in mice, pointing out that mass spectroscopy is a more reliable method, which may have produced different results in our study; however, this was not available to us.

Endocrine signaling through the FSH and insulin-like growth factor 1 (IGF1) receptors are well-known pathways that promote GC survival. Studies in animals and humans have shown that androgen signaling, both inside and outside the nucleus, can potentiate the actions of trophic growth factors in GCs and contribute to small follicle growth [60–66]. In larger follicles, androgens reduce aromatase activity [61] and promote apoptosis [67], which can be detrimental in states of androgen excess, such as polycystic ovary syndrome [68, 69]. These effects are thought to be due to androgen signaling in GCs. In fact, GC-specific androgen receptor knockout results in accelerated follicle depletion and premature ovarian failure in mice due to increased follicle apoptosis [70]. Recent studies showed that paxillin is a novel mediator of androgen receptor signaling in reproductive tissues. In prostate cancer cells, paxillin promotes both nuclear and cytoplasmic androgen actions, leading to cell proliferation, migration, and invasion [33–36]. As in other tissues, paxillin has anti-apoptotic effects in prostate cancer cells [28]. Further studies of the relationship between paxillin and androgen actions in GCs may help understand the complex role of androgens in female reproduction.

Many factors that determine female fertility have yet to be examined in relation to paxillin. GC communications to oocytes can translate into oocyte quality: for example, aromatase activity in cumulus GCs has been linked to oocyte maturation in preovulatory follicles [71]. We have not yet investigated whether paxillin loss in GCs affects oocyte quality. Paxillin can regulate DNA methylation, leading to changes in gene expression. GC DNA methylation patterns change with aging, resulting in altered expression of key GC genes, including AMH [72]. We have not yet examined whether paxillin loss in our mouse model affects DNA methylation of GC genes. Gremlin 2 (GREM2), an antagonist of bone morphogenetic

protein (BMP) signaling, is required for female fertility. Global knockout of GREM2 resulted in reduced fecundity and was identified as a rare gene variant associated with POI [73]. The GREM2 knockout female fertility phenotype is in many ways the opposite of the GC-PXN KO phenotype. Another GC-specific transcription coactivator, TATA-box binding protein associated factor 4b (TAF4b), protects GCs from apoptosis and contributes to the maintenance of follicle reserve [74]. The mRNA expression levels of some of these factors were not altered in our PXN-KO GCs (Figure S4). It remains to be determined whether paxillin is involved in BMP signaling or interacts with TAF4b. Lastly, further studies are needed to examine the role of paxillin in GC autophagy, which may be a protective response to stress in the growing follicle to reduce follicle atresia through apoptosis [75–77].

In summary, we showed that paxillin knockout in mouse GCs leads to increased fecundity by increasing the likelihood of pregnancy in older reproductive age female mice. This may occur through reduced GC death, implicating paxillin as a novel regulator of female reproduction. Studies to investigate the mechanisms of paxillin actions in GCs may reveal novel treatment targets for age-related subfertility in women.

Acknowledgment

We thank the University of Rochester Medical Center Flow Cytometry Resource for assistance with PXN-knockout KGN cell selection. We thank the University of Virginia Ligand Assay & Analysis Core for the measurement of serum analytes.

Supplementary Material

Supplementary material is available at *BIOLRE* online.

Conflict of Interest: The authors have declared that no conflict of interest exists.

Authors' contributions

KV: mouse breeding and genotyping, estrous cycle studies, follicle counting, western blotting, migration assays, TUNEL assays, and manuscript preparation.
AEW: mouse breeding and genotyping, estrous cycle studies, generation of KGN PXN-KO clones, and cell proliferation assays.
ACW: mouse breeding and genotyping, immunohistochemistry.
OA: experimental design, ovulation counting, data analysis, and manuscript preparation.

Data availability

All data are available upon request from the corresponding author.

References

1. Mathews TJ, Hamilton BE. Mean age of mothers is on the rise: United States, 2000-2014. *NCHS Data Brief* 2016; **232**:1–8.
2. Nelson SM, Telfer EE, Anderson RA. The ageing ovary and uterus: new biological insights. *Hum Reprod Update* 2013; **19**:67–83.
3. Demko ZP, Simon AL, McCoy RC, Petrov DA, Rabinowitz M. Effects of maternal age on euploidy rates in a large cohort of embryos analyzed with 24-chromosome single-nucleotide polymorphism-based preimplantation genetic screening. *Fertil Steril* 2016; **105**:1307–1313.
4. Bentov Y, Yavorska T, Esfandiari N, Jurisicova A, Casper RF. The contribution of mitochondrial function to reproductive aging. *J Assist Reprod Genet* 2011; **28**:773–783.
5. Meldrum DR, Casper RF, Diez-Juan A, Simon C, Domar AD, Frydman R. Aging and the environment affect gamete and embryo potential: can we intervene? *Fertil Steril* 2016; **105**:548–559.
6. Yang H, Xie Y, Yang D, Ren D. Oxidative stress-induced apoptosis in granulosa cells involves JNK, p53 and Puma. *Oncotarget* 2017; **8**:25310–25322.
7. Lim J, Luderer U. Oxidative damage increases and antioxidant gene expression decreases with aging in the mouse ovary. *Biol Reprod* 2011; **84**:775–782.
8. Yan F, Zhao Q, Li Y, Zheng Z, Kong X, Shu C, Liu Y, Shi Y. The role of oxidative stress in ovarian aging: a review. *J Ovarian Res* 2022; **15**:100.
9. Liang X, Yan Z, Ma W, Qian Y, Zou X, Cui Y, Liu J, Meng Y. Peroxiredoxin 4 protects against ovarian ageing by ameliorating D-galactose-induced oxidative damage in mice. *Cell Death Dis* 2020; **11**:1053.
10. Fan Y, Chang Y, Wei L, Chen J, Li J, Goldsmith S, Silber S, Liang X. Apoptosis of mural granulosa cells is increased in women with diminished ovarian reserve. *J Assist Reprod Genet* 2019; **36**:1225–1235.
11. Seifer DB, Gardiner AC, Ferreira KA, Peluso JJ. Apoptosis as a function of ovarian reserve in women undergoing in vitro fertilization. *Fertil Steril* 1996; **66**:593–598.
12. Sadraie SH, Saito H, Kaneko T, Saito T, Hiroi M. Effects of aging on ovarian fecundity in terms of the incidence of apoptotic granulosa cells. *J Assist Reprod Genet* 2000; **17**:168–173.
13. Oosterhuis GJ, Michgelsen HW, Lambalk CB, Schoemaker J, Vermes I. Apoptotic cell death in human granulosa-lutein cells: a possible indicator of in vitro fertilization outcome. *Fertil Steril* 1998; **70**:747–749.
14. Nakahara K, Saito H, Saito T, Ito M, Ohta N, Sakai N, Tezuka N, Hiroi M, Watanabe H. Incidence of apoptotic bodies in membrana granulosa of the patients participating in an in vitro fertilization program. *Fertil Steril* 1997; **67**:302–308.
15. Huang Y, Hu C, Ye H, Luo R, Fu X, Li X, Huang J, Chen W, Zheng Y. Inflamm-aging: A new mechanism affecting premature ovarian insufficiency. *J Immunol Res* 2019; **2019**:8069898.
16. Kasapoglu I, Seli E. Mitochondrial dysfunction and ovarian aging. *Endocrinology* 2020; **161**:2.
17. Lin N, Lin J, Plosch T, Sun P, Zhou X. An oxidative stress-related gene signature in granulosa cells is associated with ovarian aging. *Oxid Med Cell Longev* 2022; **2022**:1070968.
18. Turner CE, Glenney JR Jr, Burridge K. Paxillin: a new vinculin-binding protein present in focal adhesions. *J Cell Biol* 1990; **111**:1059–1068.
19. Brown MC, Turner CE. Paxillin: adapting to change. *Physiol Rev* 2004; **84**:1315–1339.
20. Lopez-Colome AM, Lee-Rivera I, Benavides-Hidalgo R, López E. Paxillin: a crossroad in pathological cell migration. *J Hematol Oncol* 2017; **10**:50.
21. Song SH, Lee KH, Kang MS, Lee YJ. Role of paxillin in metabolic oxidative stress-induced cytoskeletal reorganization: involvement of SAPK signal transduction pathway and PTP-PEST gene expression. *Free Radic Biol Med* 2000; **29**:61–70.
22. Deakin NO, Turner CE. Distinct roles for paxillin and Hic-5 in regulating breast cancer cell morphology, invasion, and metastasis. *Mol Biol Cell* 2011; **22**:327–341.
23. Turner CE. Paxillin interactions. *J Cell Sci* 2000; **113**:4139–4140.
24. Ma X, Hammes SR. Paxillin actions in the nucleus. *Steroids* 2018; **133**:87–92.
25. Chay KO, Park SS, Mushinski JF. Linkage of caspase-mediated degradation of paxillin to apoptosis in Ba/F3 murine pro-B lymphocytes. *J Biol Chem* 2002; **277**:14521–14529.
26. Shim SR, Kook S, Kim JI, Song WK. Degradation of focal adhesion proteins paxillin and p130cas by caspases or calpains in apoptotic

rat-1 and L929 cells. *Biochem Biophys Res Commun* 2001; **286**: 601–608.
27. Alpha KM, Xu W, Turner CE. Paxillin family of focal adhesion adaptor proteins and regulation of cancer cell invasion. *Int Rev Cell Mol Biol* 2020; **355**:1–52.
28. Xiao P, Ma T, Zhou C, Xu Y, Liu Y, Zhang H. Anticancer effect of docetaxel induces apoptosis of prostate cancer via the cofilin-1 and paxillin signaling pathway. *Mol Med Rep* 2016; **13**:4079–4084.
29. Gawlak G, Tian Y, O'Donnell JJ III, Tian X, Birukova AA, Birukov KG. Paxillin mediates stretch-induced Rho signaling and endothelial permeability via assembly of paxillin-p42/44MAPK-GEF-H1 complex. *FASEB J* 2014; **28**:3249–3260.
30. McGinnis LK, Kinsey WH. Role of focal adhesion kinase in oocyte-follicle communication. *Mol Reprod Dev* 2015; **82**:90–102.
31. Kitasaka H, Kawai T, Hoque SAM, Umehara T, Fujita Y, Shimada M. Inductions of granulosa cell luteinization and cumulus expansion are dependent on the fibronectin-integrin pathway during ovulation process in mice. *PloS One* 2018; **13**:e0192458.
32. Tian Y, Zhang MY, Li N, Wang JJ, Ge W, Tan SJ, Shen W, Li L. Zearalenone exposure triggered porcine granulosa cells apoptosis via microRNAs-mediated focal adhesion pathway. *Toxicol Lett* 2020; **330**:80–89.
33. Ma X, Biswas A, Hammes SR. Paxillin regulated genomic networks in prostate cancer. *Steroids* 2019; **151**:108463.
34. Sen A, O'Malley K, Wang Z, Raj GV, DeFranco DB, Hammes SR. Paxillin regulates androgen- and epidermal growth factor-induced MAPK signaling and cell proliferation in prostate cancer cells. *J Biol Chem* 2010; **285**:28787–28795.
35. Kasai M, Guerrero-Santoro J, Friedman R, Leman ES, Getzenberg RH, DeFranco D. The Group 3 LIM domain protein paxillin potentiates androgen receptor transactivation in prostate cancer cell lines. *Cancer Res* 2003; **63**:4927–4935.
36. Sen A, de Castro I, DeFranco DB, Deng FM, Melamed J, Kapur P, Raj GV, Rossi R, Hammes SR. Paxillin mediates extranuclear and intranuclear signaling in prostate cancer proliferation. *J Clin Invest* 2012; **122**:2469–2481.
37. Sen A, Prizant H, Light A, Biswas A, Hayes E, Lee HJ, Barad D, Gleicher N, Hammes SR. Androgens regulate ovarian follicular development by increasing follicle stimulating hormone receptor and microRNA-125b expression. *Proc Natl Acad Sci U S A* 2014; **111**:3008–3013.
38. Grossman H, Chuderland D, Ninio-Many L, Hasky N, Kaplan-Kraicer R, Shalgi R. A novel regulatory pathway in granulosa cells, the LH/human chorionic gonadotropin-microRNA-125a-3p-Fyn pathway, is required for ovulation. *FASEB J* 2015; **29**: 3206–3216.
39. Rashid M, Belmont J, Carpenter D, Turner CE, Olson EC. Neural-specific deletion of the focal adhesion adaptor protein paxillin slows migration speed and delays cortical layer formation. *Development* 2017; **144**:4002–4014.
40. Jorgez CJ, Klysik M, Jamin SP, Behringer RR, Matzuk MM. Granulosa cell-specific inactivation of follistatin causes female fertility defects. *Mol Endocrinol* 2004; **18**:953–967.
41. Byers SL, Wiles MV, Dunn SL, Taft RA. Mouse estrous cycle identification tool and images. *PloS One* 2012; **7**:e35538.
42. McLean AC, Valenzuela N, Fai S, Bennett SAL. Performing vaginal lavage, crystal violet staining, and vaginal cytological evaluation for mouse estrous cycle staging identification. *J Vis Exp* 2012; **67**:e4389.
43. Myers M, Britt KL, Wreford NGM, Ebling FJP, Kerr JB. Methods for quantifying follicular numbers within the mouse ovary. *Reproduction* 2004; **127**:569–580.
44. Tian Y, Shen W, Lai Z, Shi L, Yang S, Ding T, Wang S, Luo A. Isolation and identification of ovarian theca-interstitial cells and granulose cells of immature female mice. *Cell Biol Int* 2015; **39**: 584–590.
45. Astapova O, Seger C, Hammes SR. Ligand binding prolongs androgen receptor protein half-life by reducing its degradation. *J Endocr Soc* 2021; **5**:bvab035.
46. Schneider CA, Rasband WS, Eliceiri KW. NIH Image to ImageJ: 25 years of image analysis. *Nat Methods* 2012; **9**:671–675.
47. Zaqout S, Becker LL, Kaindl AM. Immunofluorescence staining of paraffin sections step by step. *Front Neuroanat* 2020; **14**:582218.
48. Kevenaar ME, Meerasahib MF, Kramer P, van de Lang-Born BMN, de Jong FH, Groome NP, Themmen APN, Visser JA. Serum anti-mullerian hormone levels reflect the size of the primordial follicle pool in mice. *Endocrinology* 2006; **147**:3228–3234.
49. Moore CL, Savenka AV, Basnakian AG. TUNEL assay: a powerful tool for kidney injury evaluation. *Int J Mol Sci* 2021; **22**:412.
50. O'Shea JD, Rodgers RJ, D'Occhio MJ. Cellular composition of the cyclic corpus luteum of the cow. *J Reprod Fertil* 1989; **85**:483–487.
51. Shi L, Zhang J, Lai Z, Tian Y, Fang L, Wu M, Xiong J, Qin X, Luo A, Wang S. Long-term moderate oxidative stress decreased ovarian reproductive function by reducing follicle quality and progesterone production. *PloS One* 2016; **11**:e0162194.
52. Huang F, Wang P, Wang X. Thapsigargin induces apoptosis of prostate cancer through cofilin-1 and paxillin. *Oncol Lett* 2018; **16**:1975–1980.
53. Huang SM, Hsu PC, Chen MY, Li WS, More SV, Lu KT, Wang YC. The novel indole compound SK228 induces apoptosis and FAK/Paxillin disruption in tumor cell lines and inhibits growth of tumor graft in the nude mouse. *Int J Cancer* 2012; **131**:722–732.
54. Nah AS, Chay KO. Roles of paxillin phosphorylation in IL-3 withdrawal-induced Ba/F3 cell apoptosis. *Genes Genomics* 2019; **41**:241–248.
55. Niu M, Nachmias VT. Increased resistance to apoptosis in cells overexpressing thymosin beta four: a role for focal adhesion kinase pp125FAK. *Cell Adhes Commun* 2000; **7**:311–320.
56. van de Water B, Houtepen F, Huigsloot M, Tijdens IB. Suppression of chemically induced apoptosis but not necrosis of renal proximal tubular epithelial (LLC-PK1) cells by focal adhesion kinase (FAK). Role of FAK in maintaining focal adhesion organization after acute renal cell injury. *J Biol Chem* 2001; **276**:36183–36193.
57. Cimino I, Casoni F, Liu X, Messina A, Parkash J, Jamin SP, Catteau-Jonard S, Collier F, Baroncini M, Dewailly D, Pigny P, Prescott M, *et al.* Novel role for anti-Mullerian hormone in the regulation of GnRH neuron excitability and hormone secretion. *Nat Commun* 2016; **7**:10055.
58. Ferdousy RN, Kereilwe O, Kadokawa H. Anti-Mullerian hormone receptor type 2 (AMHR2) expression in bovine oviducts and endometria: comparison of AMHR2 mRNA and protein abundance between old Holstein and young and old Wagyu females. *Reprod Fertil Dev* 2020; **32**:738–747.
59. Ghosh A, Syed SM, Kumar M, Carpenter TJ, Teixeira JM, Houairia N, Negi S, Tanwar PS. In vivo cell fate tracing provides no evidence for mesenchymal to epithelial transition in adult fallopian tube and uterus. *Cell Rep* 2020; **31**:107631.
60. Nandedkar TD, Munshi SR. Effect of dihydrotestosterone on follicular development, ovulation and reproductive capacity of mice. *J Reprod Fertil* 1981; **62**:21–24.
61. Hillier SG, Tetsuka M. Role of androgens in follicle maturation and atresia. *Baillieres Clin Obstet Gynaecol* 1997; **11**:249–260.
62. Vendola K, Zhou J, Wang J, Bondy CA. Androgens promote insulin-like growth factor-I and insulin-like growth factor-I receptor gene expression in the primate ovary. *Hum Reprod* 1999; **14**: 2328–2332.
63. Weil S, Vendola K, Zhou J, Bondy CA. Androgen and follicle-stimulating hormone interactions in primate ovarian follicle development. *J Clin Endocrinol Metab* 1999; **84**:2951–2956.
64. Gervásio CG, Bernuci MP, Silva-de-Sá MF, Rosa-E-Silva AC. The role of androgen hormones in early follicular development. *ISRN Obstet Gynecol* 2014; **2014**:818010.
65. Baumgarten SC, Armouti M, Ko CM, Stocco C. IGF1R expression in ovarian granulosa cells is essential for steroidogenesis, follicle survival, and fertility in female mice. *Endocrinology* 2017; **158**: 2309–2318.
66. Laird M, Thomson K, Fenwick M, Mora J, Franks S, Hardy K. Androgen stimulates growth of mouse preantral follicles in vitro:

interaction with follicle-stimulating hormone and with growth factors of the TGFbeta superfamily. *Endocrinology* 2017; **158**: 920–935.
67. Franks S, Hardy K. Androgen action in the ovary. *Front Endocrinol (Lausanne)* 2018; **9**:452.
68. Salehi R, Mazier HL, Nivet AL, Reunov AA, Lima P, Wang Q, Fiocco A, Isidoro C, Tsang BK. Ovarian mitochondrial dynamics and cell fate regulation in an androgen-induced rat model of polycystic ovarian syndrome. *Sci Rep* 2020; **10**:1021.
69. Lima PDA, Nivet AL, Wang Q, Chen YA, Leader A, Cheung A, Tzeng CR, Tsang BK. Polycystic ovary syndrome: possible involvement of androgen-induced, chemerin-mediated ovarian recruitment of monocytes/macrophages. *Biol Reprod* 2018; **99**:838–852.
70. Sen A, Hammes SR. Granulosa cell-specific androgen receptors are critical regulators of ovarian development and function. *Mol Endocrinol* 2010; **24**:1393–1403.
71. Polan ML, Laufer N, Ohkawa R, Botero-Ruiz W, Haseltine FP, DeCherney AH, Behrman HR. The association between granulosa cell aromatase activity and oocyte-corona-cumulus-complex maturity from individual human follicles. *J Clin Endocrinol Metab* 1984; **59**:170–174.
72. Yu B, Russanova VR, Gravina S, Hartley S, Mullikin JC, Ignezweski A, Graham J, Segars JH, DeCherney AH, Howard BH. DNA methylome and transcriptome sequencing in human ovarian granulosa cells links age-related changes in gene expression to gene body methylation and 3′-end GC density. *Oncotarget* 2015; **6**: 3627–3643.
73. Rydze RT, Patton BK, Briley SM, Salazar Torralba H, Gipson G, James R, Rajkovic A, Thompson T, Pangas SA. Deletion of Gremlin-2 alters estrous cyclicity and disrupts female fertility in micedagger. *Biol Reprod* 2021; **105**:1205–1220.
74. Voronina E, Lovasco LA, Gyuris A, Baumgartner RA, Parlow AF, Freiman RN. Ovarian granulosa cell survival and proliferation requires the gonad-selective TFIID subunit TAF4b. *Dev Biol* 2007; **303**:715–726.
75. Zheng Y, Ma L, Liu N, Tang X, Guo S, Zhang B, Jiang Z. Autophagy and apoptosis of porcine ovarian granulosa cells during follicular development. *Animals (Basel)* 2019; **9**:1111.
76. Shao T, Ke H, Liu R, Xu L, Han S, Zhang X, Dang Y, Jiao X, Li W, Chen ZJ, Qin Y, Zhao S. Autophagy regulates differentiation of ovarian granulosa cells through degradation of WT1. *Autophagy* 2022; **18**:1864–1878.
77. Tang Z, Xu R, Zhang Z, Shi C, Zhang Y, Yang H, Lin Q, Liu Y, Lin F, Geng B, Wang Z. HIF-1alpha protects granulosa cells from hypoxia-induced apoptosis during follicular development by inducing autophagy. *Front Cell Dev Biol* 2021; **9**:631016.